ADVANCING EARTH AND SPACE SCIENCES

JGR Solid Earth

RESEARCH ARTICLE

10.1029/2025JB032042

The Characteristics of Rayleigh and Love Wave Azimuthal Anisotropy: Observations Across Alaska

Xiongwei Liu[1], Chuanming Liu[2], and Michael H. Ritzwoller[1]

[1]Department of Physics, University of Colorado Boulder, Boulder, CO, USA, [2]Institute for Geophysics & Department of Earth and Planetary Sciences, Jackson School of Geosciences, The University of Texas at Austin, Austin, TX, USA

Key Points:

- Rayleigh wave and Love wave 2ψ and 4ψ azimuthal anisotropy are observed from 10 to 50 s period based on ambient noise data
- Complementary patterns in 2ψ and 4ψ anisotropy between Rayleigh and Love waves arise from Rayleigh–Love coupling
- The fast orientations of various components of anisotropy are related, consistent with expectations for tilted transversely isotropic media

Supporting Information:

Supporting Information may be found in the online version of this article.

Correspondence to:

X. Liu,
Xiongwei.Liu@colorado.edu

Citation:

Liu, X., Liu, C., & Ritzwoller, M. H. (2025). The characteristics of Rayleigh and Love wave azimuthal anisotropy: Observations across Alaska. *Journal of Geophysical Research: Solid Earth*, *130*, e2025JB032042. https://doi.org/10.1029/2025JB032042

Received 27 MAY 2025
Accepted 1 NOV 2025

Author Contributions:

Conceptualization: Xiongwei Liu, Michael H. Ritzwoller
Data curation: Xiongwei Liu, Chuanming Liu
Formal analysis: Xiongwei Liu, Michael H. Ritzwoller
Funding acquisition: Michael H. Ritzwoller
Investigation: Xiongwei Liu, Michael H. Ritzwoller
Methodology: Xiongwei Liu, Chuanming Liu, Michael H. Ritzwoller
Project administration: Michael H. Ritzwoller
Resources: Michael H. Ritzwoller
Supervision: Michael H. Ritzwoller
Validation: Xiongwei Liu, Michael H. Ritzwoller
Visualization: Xiongwei Liu, Michael H. Ritzwoller
Writing – original draft: Xiongwei Liu

Abstract Using ambient noise data from 10 to 50 s period across Alaska, we confirm previous estimates of Rayleigh wave 2ψ azimuthal anisotropy and present the first estimates of Rayleigh wave 4ψ and Love wave 2ψ and 4ψ azimuthal anisotropy, where ψ is the angle of propagation. As in earlier studies, the fast orientations of Rayleigh wave 2ψ are mainly parallel to major faults in Alaska at all periods. We also find that on average the fast orientations of Love wave 4ψ are rotated 45° relative to Rayleigh wave 2ψ, the fast orientation of Rayleigh wave 4ψ aligns with Love wave 2ψ, and the fast orientation differences of Rayleigh and Love wave 2ψ range between 0° and 90° with many between 40° to 60°. These observations are consistent with non-elliptical anisotropy with the ellipticity parameters η_K and η_X considerably smaller than 1. Observations of Love wave 2ψ and Rayleigh wave 4ψ reflect strong Rayleigh-Love coupling, which causes the observed complementary trends with period of the amplitudes of Rayleigh and Love wave 2ψ and Rayleigh and Love wave 4ψ. Recent theories of Rayleigh-Love coupling based on a quasi-degenerate theory allow these observations to be understood and to be used in the future to improve models of the elastic tensor in the crust and mantle.

Plain Language Summary We conduct surface wave tomography across Alaska based on ambient noise data. We find strong directional dependence or azimuthal anisotropy of surface wave phase velocities, including both Rayleigh and Love waves. These signals arise from the coupling between Rayleigh and Love waves which is a physical interaction between the two types of surface waves caused by anisotropy. Recognizing this coupling helps to interpret seismic observations and provides a foundation for constructing more accurate seismic models of anisotropy in the future. Such models will improve our understanding of past and present deformation and dynamical processes within Alaska's lithosphere.

1. Introduction

Because surface waves propagate horizontally, surface wave phase speed in anisotropic media depends on the azimuth of propagation ψ. Smith and Dahlen (1973) demonstrated using non-degenerate perturbation theory (or Rayleigh's Principle) in which Rayleigh and Love waves interact only weakly that in a weakly anisotropic medium the azimuthal variation of Rayleigh and Love wave phase and group speeds at angular frequency ω is of the form

$$c(\psi) = c_0\left[1 + \frac{A_2}{2}\cos\left(2(\psi - \psi_2)\right) + \frac{A_4}{2}\cos 4(\psi - \psi_4)\right] \tag{1}$$

where c_0 is the isotropic speed, ψ is measured clockwise from north, ψ_2 and A_2 are the fast orientation and peak-to-peak amplitude for 2ψ, and ψ_4 and A_4 are the fast orientation and peak-to-peak amplitude for 4ψ, respectively. They argued that the azimuthal dependence of Rayleigh wave speed will be dominated by the 2ψ term in Equation 1 whereas the Love wave speeds will be dominated by the 4ψ term. Montagner and Nataf (1986) presented straightforward integral expressions so that observations of the frequency dependence of the coefficients in Equation 1 can be used to invert for the depth-dependent components of the elastic tensor. They also argued that fast orientations for the 2ψ terms for Rayleigh and Love waves should be out of phase by 90°. The observation of odd-symmetry components (e.g., 1ψ) has been explained by scattering or body-wave interference (Lin & Ritzwoller, 2011; Mauerberger et al., 2021; Zeng et al., 2024).

Based on these studies, focus has been placed on observing and interpreting the modes of anisotropy to be expected if Rayleigh and Love waves couple only weakly. These are the 2ψ component of Rayleigh wave anisotropy

10.1029/2025JB032042

Writing – review & editing:
Xiongwei Liu, Chuanming Liu, Michael H. Ritzwoller

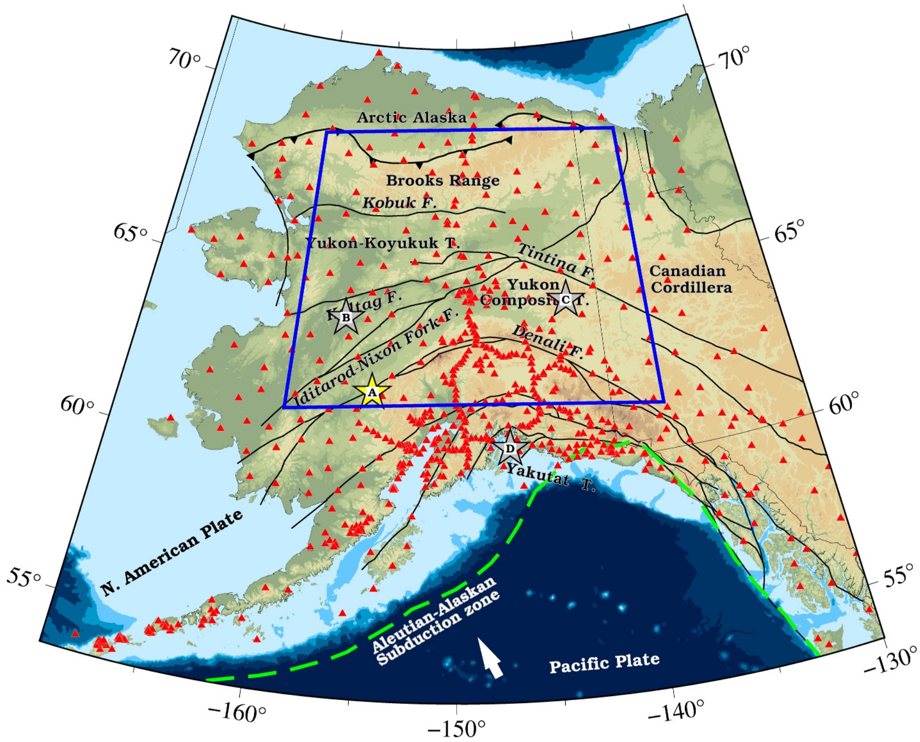

Figure 1. Seismic stations used in the study are shown with red triangles, the yellow star is Point A referred to in Figure 2, the gray stars are Point B, C, and D referred to in Figure 6, and the blue rectangle is the region used to compute the average amplitude of anisotropy in Figure 4. Black lines are major faults.

and harder to observe 4ψ component of Love wave anisotropy. Many researchers have presented and interpreted the 2ψ component of Rayleigh wave anisotropy observed with earthquake data, with studies dating back to the mid-1970s (e.g., Forsyth, 1975; Leveque et al., 1988; Montagner & Jobert, 1988; Nishimura & Forsyth, 1988; Tanimoto & Anderson, 1985, and many others). More recently, these observations have been expanded to include ambient noise observations at higher spatial resolution (e.g., Lin et al., 2011; Yao et al., 2010, and others) and full waveform inversion (e.g., Yuan & Romanowicz, 2010; Zhu & Tromp, 2013, and others). Inversions for earth structure based on 2ψ component of Rayleigh wave anisotropy have been performed to estimate apparent azimuthal anisotropy as a function of depth (Lin et al., 2011; Zhu et al., 2020) as well as inherent anisotropy represented by the elastic tensor (e.g., C. Liu & Ritzwoller, 2024; Xie et al., 2015, 2017). Observations of the 4ψ component of Love wave anisotropy are much more rare (e.g., Ekström, 2011; Montagner & Tanimoto, 1990; Russell et al., 2019; Trampert & Woodhouse, 2003; Visser et al., 2008; Yuan & Beghein, 2014).

Less effort has been devoted to observing the previously unexpected components of anisotropy, the 2ψ variation of Love wave phase speeds and the 4ψ component of the Rayleigh waves. Nevertheless, several studies have found that fundamental mode surface waves appear to possess both 2ψ and 4ψ variations with azimuth (e.g., Montagner & Tanimoto, 1990; Polat et al., 2012; Russell et al., 2019; Trampert & Woodhouse, 2003; Visser et al., 2008). Most of these studies have been performed on a global scale at long periods. In contrast, the local area study of Russell et al. (2019) was performed in a narrow short period band (5–7.5 s). Recently, X. Liu and Ritzwoller (2025) show theoretically based on a quasi-degenerate theory that Love wave 2ψ and Rayleigh wave 4ψ anisotropy, which are unexpected based on non-degenerate perturbation theory, are expected when Rayleigh-Love coupling is strong and discuss the nature of the anisotropy that will produce such coupling.

In this study, we use data from the USArray Transportable Array (TA) and regional networks across Alaska (Figure 1) to investigate the nature of surface wave anisotropy. Other studies have investigated surface wave anisotropy across Alaska before this study, but have focused on Rayleigh wave 2ψ (e.g., Feng et al., 2020; C. Liu et al., 2022a; C. Liu et al., 2024; Z. Liu et al., 2025; Wang & Tape, 2014). We focus on investigating the existence

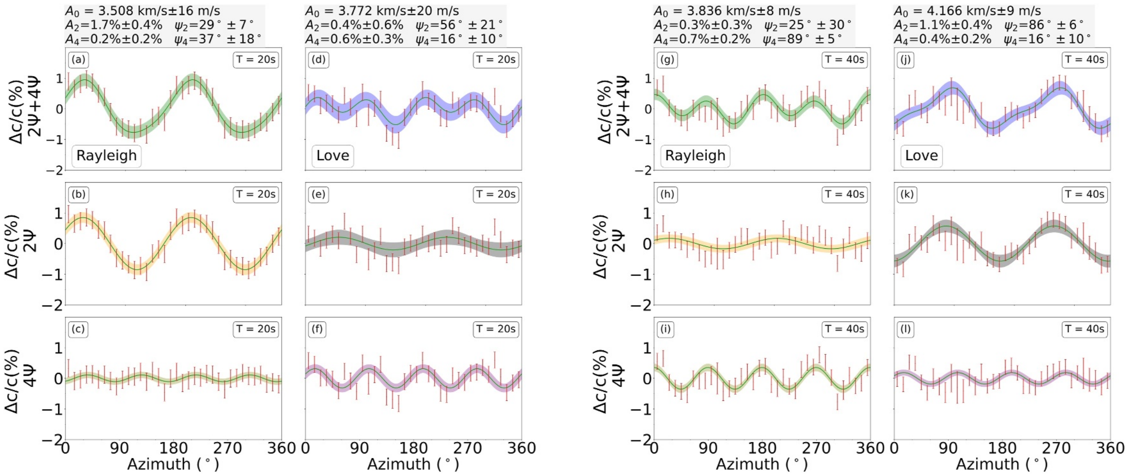

Figure 2. Examples of measurements of Rayleigh and Love anisotropy in western Alaska near the Denali fault, Location A in Figure 1. The left two columns are at 20 s period, the right two columns are at 40 s. Columns one and three are for Rayleigh waves, and columns two and four for Love waves. The top row is the complete observation and the 2ψ and 4ψ components of anisotropy are in the middle and bottom rows, respectively. The red bars are observations displaying one standard-deviation of the mean in each of 36 azimuthal bins. The estimated amplitude and fast orientation of anisotropy are shown at the top of each panel. Each shaded corridor represents the one standard deviation uncertainty in the estimated phase speed. Other observations at Point A are shown in Figures S1–S5 in Supporting Information S1.

and nature of anisotropy previously not considered, which includes Love wave 4ψ and anisotropy previously considered to be unexpected: Love wave 2ψ and Rayleigh wave 4ψ anisotropy.

We ask four principal questions for Alaska. (a) Are the expected components of azimuthal anisotropy (Rayleigh wave 2ψ and Love wave 4ψ) observed? (b) Are the unexpected components of azimuthal anisotropy (Love wave 2ψ and Rayleigh wave 4ψ) observed? (c) Are the fast orientations of some of these observables related; in particular are the fast orientations for the 2ψ components of Rayleigh and Love waves rotated by 90° relative to each other? (d) Do the amplitudes of Rayleigh and Love wave azimuthal anisotropy vary as a function of period consistent with the existence of Rayleigh-Love coupling? In addressing these questions, we will focus on the observations. Further discussion of their meaning for earth structure will be the subject of a later contribution.

2. Data and Methods

We use the ambient noise database constructed by C. Liu et al. (2022a), including Rayleigh and Love waves from 10 to 50 s, as input for the tomography and subsequent analysis. This database includes both traditional two-station ambient noise interferometry (Bensen et al., 2007) and the more recently developed three-station interferometry method (Zhang et al., 2020, 2021). The tomography and observational methods are discussed in Text S1 in Supporting Information S1 and methods to estimate uncertainty are discussed in Text S4 in Supporting Information S1. These methods are similar to those applied by C. Liu et al. (2022a), but here we use 36 azimuthal bins rather than 18.

Examples of measurements of the azimuthal variation of Rayleigh and Love wave phase speed at periods of 20 and 40 s for a location in western Alaska near the Denali fault (Point A of Figure 1) are shown in Figure 2. At 20 s period, anisotropy is similar to what is expected in the absence of Rayleigh-Love coupling: the Rayleigh wave mainly displays 2ψ anisotropy (Figure 2a) and the Love wave mainly 4ψ anisotropy (Figure 2d). However, at longer periods (e.g., 40 s), which are more sensitive to the mantle, the Rayleigh wave mainly shows 4ψ anisotropy (Figure 2g) and the Love wave mainly 2ψ anisotropy (Figure 2j). This result is an example of the effect of Rayleigh-Love coupling through anisotropy as discussed by X. Liu and Ritzwoller (2025).

3. Results and Discussion

Results for azimuthal anisotropy are summarized in Figure 3 at two different periods, one that is mainly sensitive to the crust (20 s) and the other that is principally sensitive to the uppermost mantle (40 s). Expected anisotropy (Rayleigh wave 2ψ and Love wave 4ψ) is presented in the first two rows and unexpected anisotropy (Love wave 2ψ and Rayleigh wave 4ψ) appears in the bottom two rows. Results and comparisons at other periods are also

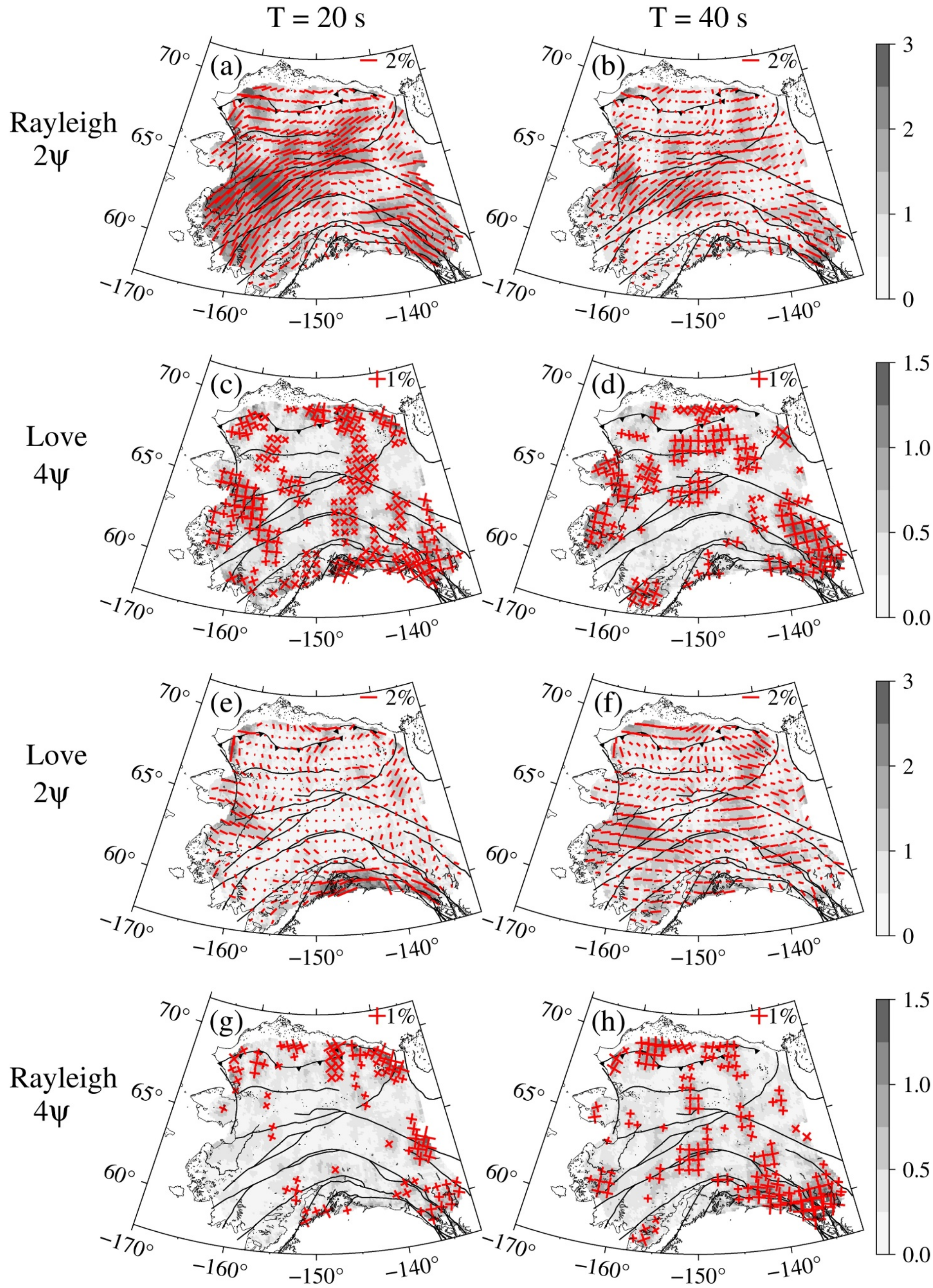

Figure 3. The amplitude and fast orientation of Rayleigh (rows 1 and 4) and Love (rows 2 and 3) wave 2ψ and 4ψ azimuthal anisotropy at periods of 20 s (left column) and 40 s (right column). The red bars indicate the fast orientation for 2ψ or fast orientations for 4ψ, with length proportional to amplitude as shown in each panel. The background gray-shade is the amplitude of the specified component of anisotropy, with units of percent of isotropic phase speed at each location. To reduce clutter, red crosses are shown for 4ψ anisotropy only when the amplitude is larger than 0.5%, which are the major signals.

shown in Figure S6–S8 in Supporting Information S1. Maps of the uncertainty in the isotropic phase speed, fast orientations, amplitude, and the amplitude of each component of anisotropy normalized by its uncertainty are shown in the Supplementary Materials (Figures S9–S22 in Supporting Information S1). Exemplary sensitivity kernels for different signals can be found in Figure S23 in Supporting Information S1. Here, by "amplitude" we mean the peak-to-peak amplitude (A_2 and A_4 in Equation 1). For a general anisotropic medium with 21 independent elastic components, the fast orientations of different signals (e.g., Rayleigh wave 2ψ, Love wave 2ψ, etc.) may be not be related to one another because they are determined by different independent elastic parameters (X.

Liu & Ritzwoller, 2025). However, in a tilted transversely isotropic (TTI) medium the fast orientations for different signals may have a specific relationship. We focus on discussing observational results in light of these expectations for a TTI medium.

3.1. Expected Anisotropy: Rayleigh Wave 2ψ and Love Wave 4ψ

"Expected anisotropy" dominates when Rayleigh-Love coupling is weak. The expected anisotropy for Rayleigh waves and Love waves closely mirrors the behavior of SV and SH waves, which display 2ψ and 4ψ, respectively, in the absence of SV-SH coupling (Backus, 1965). Rayleigh wave 2ψ anisotropy has been observed in many studies but Love wave 4ψ has presented a more significant observational challenge. Here, we first discuss these expected signals across Alaska, summarized in Figures 3a–3d at two periods and Figure S6 in Supporting Information S1 at other periods. We address questions #1 and #3 that motivate this study, notably whether Rayleigh wave 2ψ and Love wave 4ψ anisotropy are observed across Alaska and if the fast orientations of these two components are related.

3.1.1. Rayleigh Wave 2ψ

After simultaneously estimating the 2ψ and 4ψ components for the Rayleigh wave, our Rayleigh wave 2ψ results (Figures 3a and 3b) remain very similar to those of C. Liu et al. (2022a). The average amplitude of Rayleigh wave 2ψ (Figure 4a) diminishes with period from about 1.3% near 20 s period to about 0.8% at 40 s and longer periods. This reduction of amplitude with period is shown for point A in Figures S2–S5 in Supporting Information S1 and it is also visually apparent in Figures 3a and 3b. In contrast, the average uncertainty (Figure 4c) typically grows with period from about 0.3% to 0.4% at shorter periods to about 0.5% at 40 s and above. The uncertainties, therefore, are well below the average amplitudes at all periods (Figure S13 in Supporting Information S1).

To compute reliable spatially averaged quantities, such as those shown in Figure 4, we use a large subset of the observational data confined to the region outlined by the blue rectangle in Figure 1, rather than the entire study area. This restriction is motivated by other fact that observations outside this region may suffer from incomplete azimuthal coverage. However, this choice may lead to an underestimation of the spatially averaged amplitude of certain anisotropy signals at very short periods (e.g., 10 s in Figure S6g in Supporting Information S1).

The fast orientation of Rayleigh wave 2ψ mainly parallels major faults at all periods, which suggests that the potential cause of this strong anisotropy is fractures and cracks in the crust (e.g., Feng et al., 2020). This relatively simple fault-parallel pattern plays an important role in the comparison of Rayleigh wave to Love wave azimuthal anisotropy later in Section 3.2. The uncertainty in the fast orientation direction for Rayleigh wave 2ψ increases with period as the amplitude decreases, with an average of about 5° at 20 s period and 15° at 40 s period.

3.1.2. Love Wave 4ψ

A principal novelty of this study is the clear observation of Love wave 4ψ anisotropy over large parts of Alaska (Figures 3c and 3d), for example, Point A highlighted in Figure 2 as well as Figures S1–S5 in Supporting Information S1. Unlike 2ψ, which has two fast directions (a single bar), 4ψ exhibits four fast directions (two bars). As shown in Figures 4a and 4b, the average amplitude of Love wave 4ψ is smaller than the Rayleigh wave 2ψ at all periods. Like Rayleigh 2ψ, it diminishes with period but more weakly, from an average of about 0.5% at shorter periods to 0.4% at longer periods. The smaller amplitude of the Love wave 4ψ, particularly at longer periods, poses a challenge for its observation, in addition to the greater azimuthal resolution needed to observe it reliably. The average uncertainty (Figure 4d) is relatively flat with period, averaging between 0.4% and 0.5%. The average amplitude of the Love wave 4ψ lies closer to but still above the uncertainty level on average. The uncertainty normalized amplitude across Alaska is presented in Figure S16 in Supporting Information S1.

Largely due to limitations in azimuthal resolution, previous studies have not discussed the fast orientation of Love wave 4ψ or its comparison to Rayleigh wave 2ψ. The uncertainty of the fast orientations for Love wave 4ψ grows sightly with period from about 10° to 15° (Figure 4f) as its average amplitude decreases (Figure 4b).

Figure 5a presents the difference between the fast orientations of Love wave 4ψ (Figures 3c and 3d) at 20 s period and Rayleigh wave 2ψ (Figures 3a and 3b) at 14 s period, and Figure 5c summarizes this difference across Alaska with a histogram. These periods are chosen so that the sensitivity kernels with depth are relatively similar, both being confined to the crust (Figure S23 in Supporting Information S1). Because 4ψ anisotropy fast orientations are

10.1029/2025JB032042

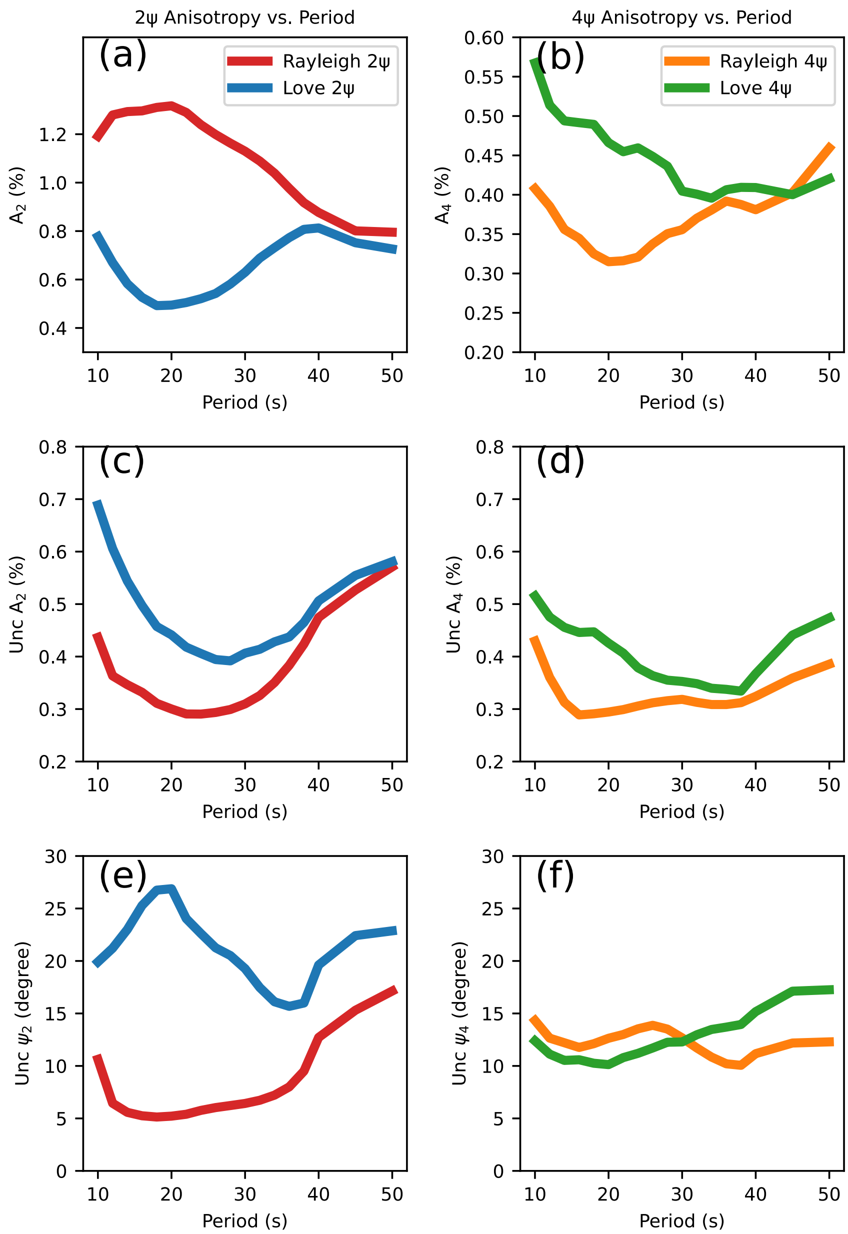

Figure 4. (a, b) Spatial average of the amplitude of Rayleigh and Love wave 2ψ and 4ψ components of anisotropy, computed within the blue rectangular box shown in Figure 1 where amplitudes are most reliable. (c–f) Uncertainty in the amplitude and fast azimuth orientations of the 2ψ and 4ψ components also computed in the blue box but with an amplitude cutoff: the uncertainty is computed only where the amplitude exceeds the spatial average.

periodic every 90°, and 2ψ anisotropy fast orientations are periodic every 180°, the absolute difference between them is restricted to the range 0°–45°. We find that the mode of the difference is about 45° (Figure 4c). Figure S7 in Supporting Information S1 presents another example histogram but for different periods (14 s for Rayleigh, 10 s for Love), which illustrates the fast orientation differences accumulating near 45° even more clearly. As discussed by X. Liu and Ritzwoller (2025), observation of a near 45° fast orientation difference indicates that the elastic tensor for a TI medium is tilted and the ellipticity parameter $\eta_X < 1$ in the crust or at least in the upper crust as Love waves are mostly sensitive to the upper crust (Figure S23 in Supporting Information S1). $\eta_X = 4L/(A + C - 2F)$, where A, C, L, and F are inherent Love moduli, and $\eta_X \approx \eta_K$ of Kawakatsu (2016). Exceptions (red colors in Figure 5a) lie near the northern and southern boundaries or where the amplitude of 4ψ is small. Locations where we do not observe the 45° difference are often associated with larger measurement uncertainties (e.g., Figure S14a in

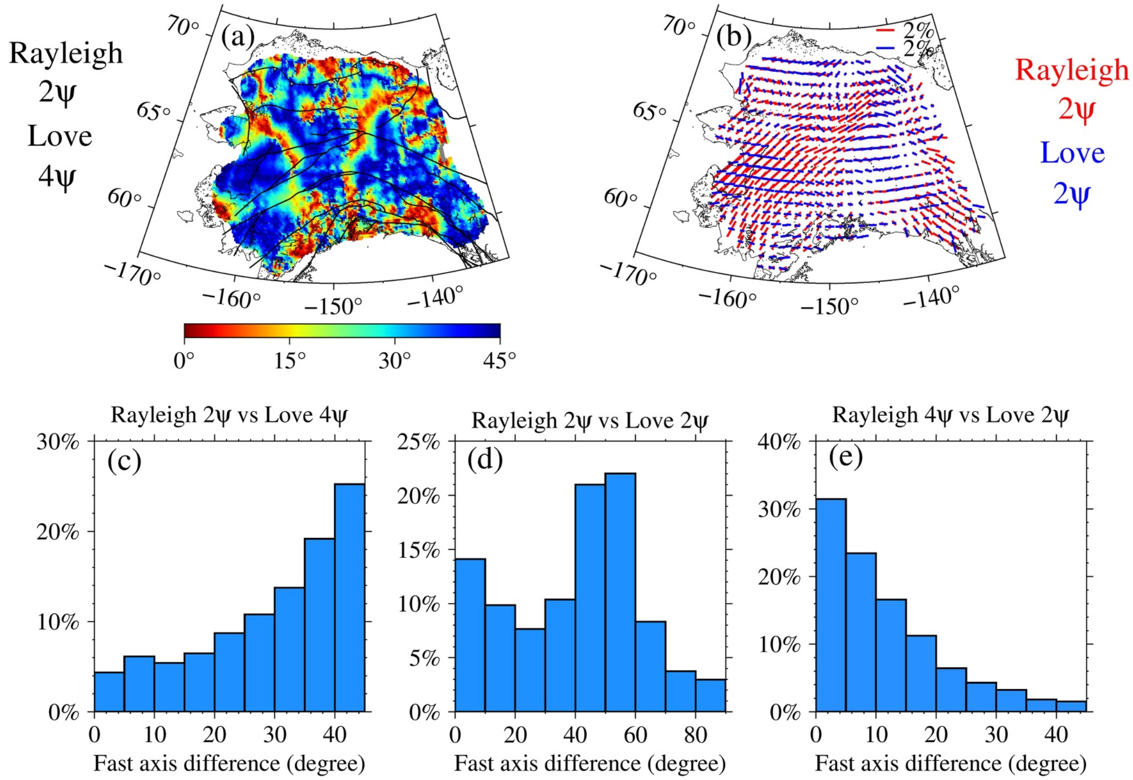

Figure 5. Comparison of fast orientations observations. Histograms are computed where the amplitude of the 2ψ component is greater than 0.5%, the amplitude of the 4ψ component is greater than 0.3%, the fast orientation uncertainty of the 2ψ component is less than 20 degrees, and the fast orientation uncertainty of the 4ψ component is less than 15 degrees. (a, c) Comparison is between Rayleigh wave 2ψ at 14 s period and Love wave 4ψ at 20 s period. (b, d) Comparison is between Rayleigh wave 2ψ at 20 s period and Love wave 2ψ at 40 s period. (e) Comparison is between the Rayleigh wave 4ψ at 45 s period and Love wave 2ψ at 40 s period.

Supporting Information S1). However, there are some regions where Rayleigh wave 2ψ and Love wave 4ψ are well determined and still quasi-parallel to each other, indicating that the ellipticity parameter $\eta_X > 1$. An example is Location A in western Alaska, with data shown in Figure 2 and Figures S1–S5 in Supporting Information S1. A recent study based on real rock samples indicates most of the crustal rocks show $\eta_K < 1$ (Figure 3 of Brownlee et al. (2017)). $\eta_K > 1$ can arise from a number of reasons, such as a high concentration of quartz (Brownlee et al., 2017). Further discussion of the ellipticity parameter, such as its application in receiver function anisotropy (e.g., Schulte-Pelkum et al., 2020), is beyond the scope of this paper.

3.2. Unexpected Anisotropy: Love Wave 2ψ and Rayleigh Wave 4ψ

As shown in Figures 2 and 3, in addition to the expected anisotropy, at some places and periods we observe Love wave 2ψ and Rayleigh wave 4ψ anisotropy, which are unexpected without Rayleigh-Love coupling. Here, we discuss the observation of these unexpected signals across Alaska, which are more prominent at the mantle-sensitive longer periods but also observed at the crust-sensitive shorter periods (e.g., Figure 6f). We address questions #2, #3, and #4 that motivate this study, notably whether Rayleigh wave 4ψ and Love wave 2ψ anisotropy are observed across Alaska, if the fast orientations of Love wave 2ψ and Rayleigh wave 2ψ and 4ψ anisotropy are related, and whether the amplitudes of Rayleigh and Love wave anisotropy vary with period consistent with Rayleigh-Love coupling.

3.2.1. Love Wave 2ψ

The principal result of this study is the observation of Love wave 2ψ anisotropy, depicted in Figures 3e, 3f and Figures S6g–S6i in Supporting Information S1. The amplitude of this signal on average grows with period from about 0.5% at 20 s period to 0.8% at 40 s period (Figure 4a). The uncertainty (Figure 4c) varies with period, but

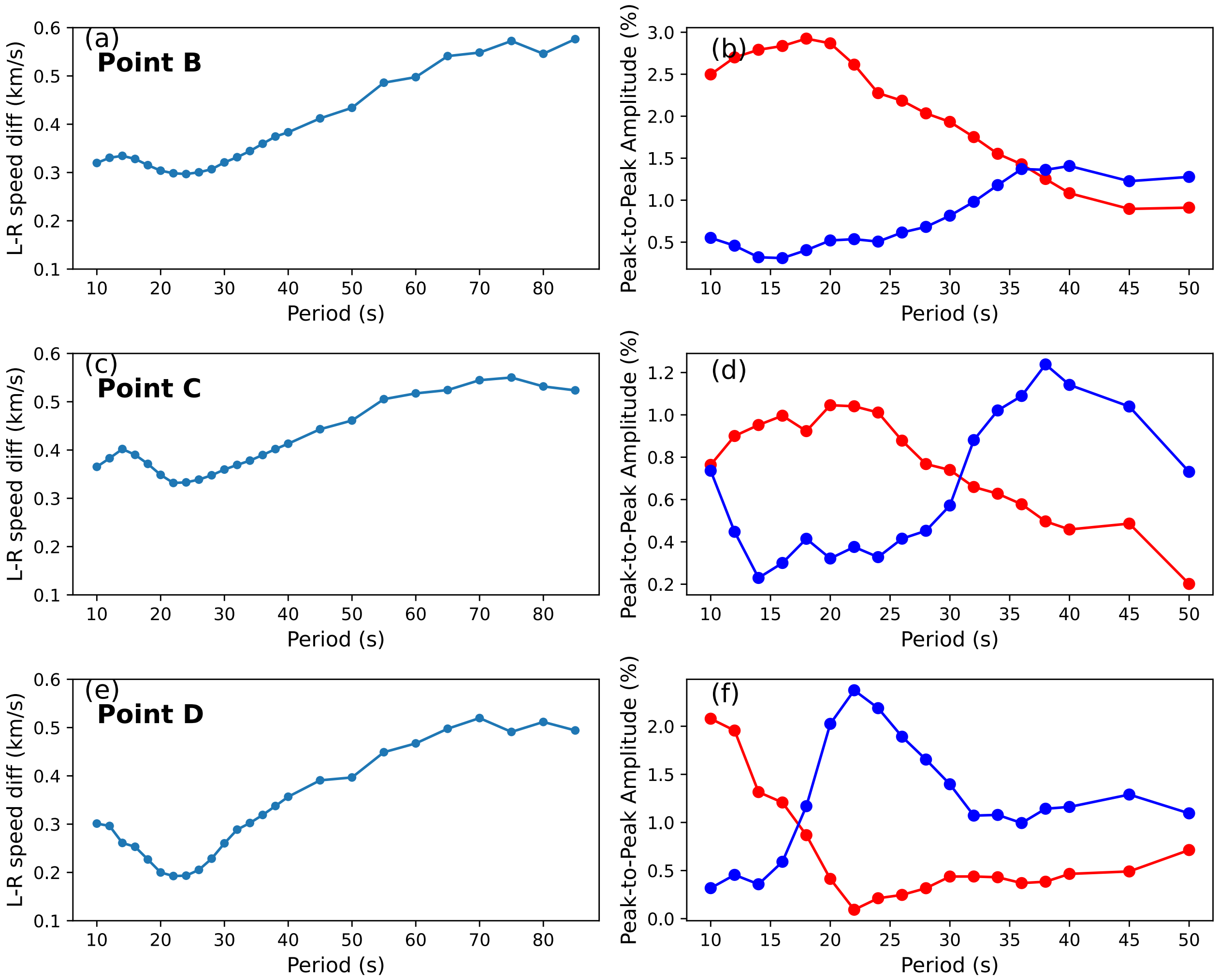

Figure 6. Observational examples of the effect of Rayleigh-Love coupling at three points identified in Figure 1: Point B (first row), Point C (second row), and Point D (third row). (a, c, e) The phase speed difference between the Rayleigh wave and Love wave at periods of 10–85 s. (b, d, f) The Rayleigh wave 2ψ amplitude (red lines) and the Love wave 2ψ amplitude (blue lines) from 10 to 50 s period. The dots are our estimated quantities. The isotropic phase speed differences larger than 50 s are based on dispersion measurements from earthquakes taken from C. Liu et al. (2022a, 2022b).

averages between 0.4% and 0.6%, so the signal is typically larger than the uncertainty at most points. The uncertainty normalized amplitude across Alaska is shown in Figure S19 in Supporting Information S1.

Figures 3a, 3b, 3e, 3f, and 4a show that the amplitude of Love wave 2ψ varies with period approximately opposite from Rayleigh wave 2ψ. A detailed local comparison of the amplitudes of Love and Rayleigh wave 2ψ is shown in Figure 6 for three points in Alaska (Points B, C, and D identified in Figure 1). These three points exemplify the spatially averaged statistics presented in Figure 4a, that the Love wave 2ψ amplitude increases and the Rayleigh wave 2ψ amplitude decreases with period (Figures 6b, 6d, and 6f) which we infer to result of Rayleigh-Love coupling. For Points B and C, Rayleigh-Love coupling is mainly caused by anisotropy in the mantle. For Point D, when the isotropic phase speed difference minimizes between 20 and 30 s period (Figure 6e), the amplitude of Rayleigh wave 2ψ decreases rapidly while the amplitude of Love wave 2ψ increases (Figure 6f). X. Liu and Ritzwoller (2025) discuss that this is the hallmark of Rayleigh-Love coupling, where the energy of the Rayleigh wave, which is strong at shorter periods, is transmitted to the Love wave through anisotropy coupling at the longer periods. The phase speeds of the Rayleigh and Love waves at Point D are similar enough between 20 and 30 s period (Figure 6e) that a small inherent anisotropy of between 4% and 6% in the crust can cause strong Rayleigh-Love coupling and the large observed amplitude of Love wave 2ψ (Figure 6f). Details about the inversion for the depth varying elastic-tensor at these points will be presented in a later contribution.

These points are examples of common observations across Alaska (Figure 4a). For some regions in Alaska, the increase of Love wave 2ψ amplitude is not accompanied with a decrease of Rayleigh wave 2ψ amplitude and they may both increase with period. This may also result from Rayleigh-Love coupling as explained in X. Liu and Ritzwoller (2025). Nevertheless, we find that on average their amplitudes are complementary across Alaska (Figure 4a).

As with all of the fast orientation measurements, the Love wave 2ψ fast orientation uncertainty (e.g., Figure S17c in Supporting Information S1) is strongly anti-correlated with its amplitude (e.g., Figure 3f); that is, when the amplitude is high the fast orientation uncertainty falls. The fast orientation uncertainty for Love wave 2ψ lies between 15° and 25°, which is considerably larger than the uncertainty for the Rayleigh wave 2ψ. This partially reflects the higher noise level on the *T-T* component compared to the *Z-Z* component of ambient noise cross-correlations, but also that the Rayleigh 2ψ has a larger amplitude, particularly at shorter periods. Love wave 2ψ fast orientation uncertainties are larger than those of Love wave 4ψ because its azimuthal wavelength is longer by a factor of two (180 vs. 90°), so relative uncertainties are about the same.

Figure 5b overplots the Rayleigh and Love wave 2ψ fast orientations at 20 and 40 s period, respectively. We choose 20 s for the Rayleigh wave rather than 40 s for comparison because the Rayleigh wave 2ψ amplitude is stronger at 20s period, but its fast orientation directions change little between 20 s (Figure 3a) and 40 s (Figure 3b). In some places in Alaska, particularly in eastern Alaska as Figure 5b illustrates, the fast orientations are approximately parallel to one another, but more commonly they differ by an angle between 40° and 60°, which occurs across much of western Alaska. This is also reflected in the histogram shown in Figure 5d. The relationship between Rayleigh and Love wave 2ψ fast orientations is not simple, therefore, and we turn to theory to explain the observations.

For very weak Rayleigh-Love coupling, Montagner and Nataf (1986) argued that the 2ψ fast orientations for Rayleigh and Love waves should be out of phase by about 90° when they are sensitive to similar depths. Thus, absent strong Rayleigh-Love coupling, the Rayleigh wave 2ψ fast orientations would be nearly perpendicular to the Love wave 2ψ fast orientations. With strong Rayleigh-Love coupling, however, X. Liu and Ritzwoller (2025) showed that when the strike of anisotropy is constant with depth, the Love wave 2ψ fast orientations should align with the strike of anisotropy whereas the Rayleigh 2ψ fast orientations could align with the strike or be perpendicular to it. Thus, angle difference between the Rayleigh and Love wave 2ψ fast orientations could be either 0° (parallel) or 90° (perpendicular) if the strike of anisotropy is depth-invariant. In fact, we see neither the single peak (either 0° or 90°) or bimodal (0° and 90°) distributions of fast orientation differences predicted if Rayleigh-Love coupling is strong and strike is depth-invariant nor the single 90 ° difference predicted with weak Rayleigh-Love coupling (Figure 5d). We believe the reason for this is due to a significant variation in the strike of anisotropy with depth from the crust to the mantle.

To illustrate the effect of a strike variation with depth we use two synthetic TTI models (Figures 7c–7g), one with a constriant strike angle with depth and another where the strike angle differs in the crust and mantle (Figure 7g). Other aspects of the models are the same: they have a depth-constant dip angle (45°, Figure 7d), an almost constant radial anisotropy (12%, Figure 7e), and different η_X in the crust and mantle (Figure 7f). Both have a strike angle of 30° in the crust, but one continues that strike angle in the mantle and the other has a strike angle of 85° in the mantle (Figure 7g). η_X in the crust differs from 1 which makes the Rayleigh wave 2ψ fast orientation perpendicular to the strike in the crust, as discussed by Xie et al. (2015).

Figures 7a and 7b show examples of the fast orientations predicted by the theory of X. Liu and Ritzwoller (2025) with strong Rayleigh-Love coupling. With a constant strike angle with depth, the Love wave 2ψ fast orientation is the same as the strike direction at all depths. At long periods (>30 s), the Rayleigh wave 2ψ fast orientation aligns with the Love wave 2ψ fast orientation, but at short periods it is perpendicular to it. Thus, with a constant strike angle with depth, the difference between the Rayleigh and Love wave 2ψ fast orientations bifurcates to be either 0° or 90° (red line, Figure 7b). This is not what we observe, however (Figure 5d). Letting the strike angle vary from the crust to mantle, produces a strike angle difference intermediate between 0° and 90° (blue line, Figure 7b), similar to our observations. We conclude, therefore, that observed strike angle differences between Rayleigh wave 2ψ and Love wave 2ψ are evidence for strike variations with depth. The assumption in this analysis is that we only consider the coupling between the fundamental mode Rayleigh wave and the fundamental mode Love wave (X. Liu & Ritzwoller, 2025). We believe our conclusion will hold generally, however.

10.1029/2025JB032042

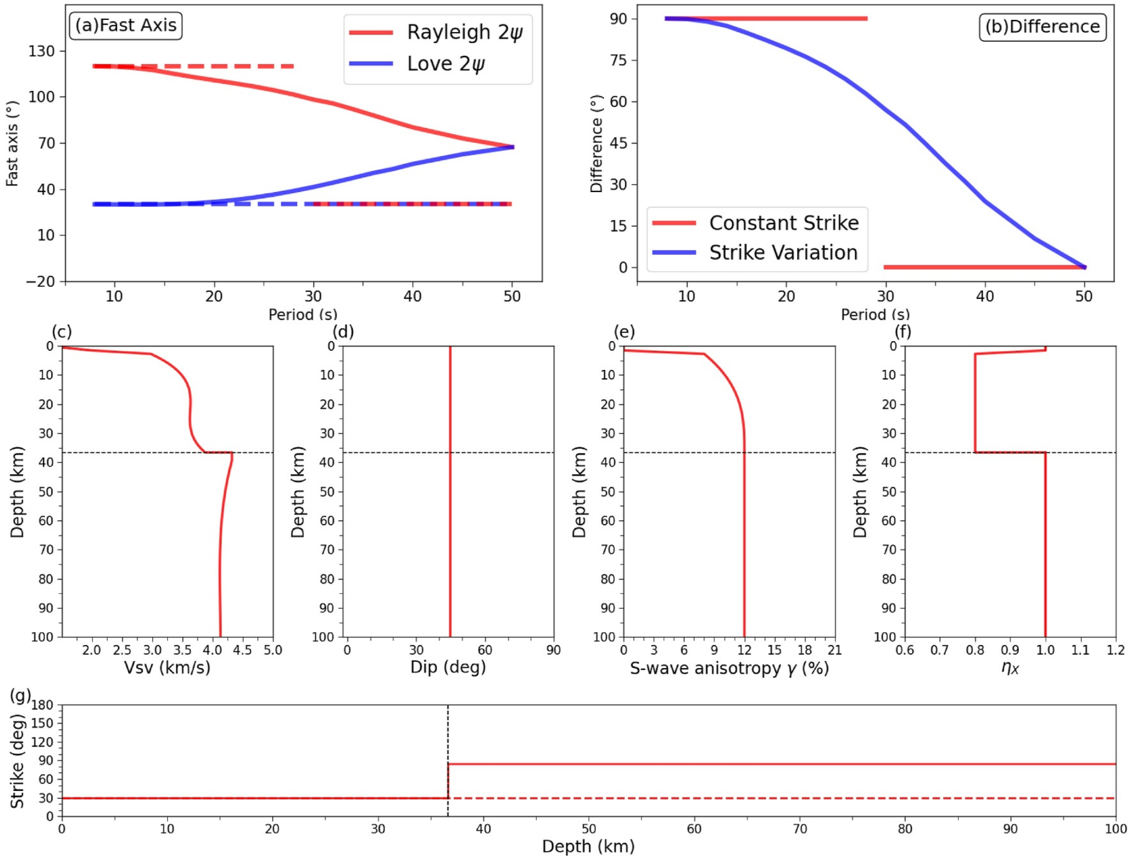

Figure 7. Synthetic test of the effect of strike variation with depth on fast-orientations. Two models, aspects of which are shown in (c)–(g), differ only in the strike angle of anisotropy. (a) Fast orientations predictions (X. Liu & Ritzwoller, 2025) for Rayleigh 2ψ (red line) and Love 2ψ (blue line) using the two models: solid line (variable strike with depth) and dashed line (constant strike with depth). (b) The fast orientation difference between Rayleigh 2ψ and Love 2ψ for the two models of strike variation with depth. (c–g) Aspects of the model used to produce the synthetic results: (c) $V_{sv} = \sqrt{L/\rho}$, (d) dip angle, (e) radial anisotropy $\gamma = (N - L)/2L$, (f) the ellipticity parameter η_X, and (g) strike angle (dashed line constant strike, solid line variable strike), where L and N are the inherent Love shear moduli. Details about the definitions can be found in Xie et al. (2015) and X. Liu and Ritzwoller (2025).

In conclusion, our observation of intermediate fast orientations differences (40°–60°, Figures 5b–5d) in western Alaska is diagnostic of a strike variation with depth. We refer to this as the fast orientations being "quasi-perpendicular." On average, therefore, Rayleigh and Love wave 2ψ fast orientations are approximately quasi-perpendicular across western Alaska and they are approximately parallel across much of eastern Alaska. Thus, strike angles are more likely to vary between the crust and mantle only subtly with depth across eastern Alaska with stronger variation with depth in western Alaska. A recent SKS study (Yang, 2021; Figure 4) identified strong azimuthal variations in some regions of western Alaska, whereas such variations were largely absent in eastern Alaska. This study may partially support our surface wave results.

Figure S8 in Supporting Information S1 presents another example histogram but for different periods (60 s for Rayleigh, 40 s for Love). This illustrates a stronger bifurcation of the fast orientations differences near 0° and 90°, which suggests a more subtle strike variation with depth.

3.2.2. Rayleigh Wave 4ψ

Although Trampert and Woodhouse (2003) argued that Rayleigh wave 4ψ should be observable, it has been largely overlooked in studies of anisotropy. We observe Rayleigh wave 4ψ across substantial parts of Alaska at longer periods, as shown in Figures 3g, and 3h, Figure S6l in Supporting Information S1, and also in Figure 2 for a single location. Rayleigh wave 4ψ is not as strong or ubiquitous as the other components in Alaska, averaging between 0.3% and 0.45% in amplitude (Figure 4b). The uncertainty in the amplitude of Rayleigh wave 4ψ averages between 0.3% and 0.4% (Figure 4d), which is smaller than the observed signal, on average, principally at the long periods. The uncertainty normalized amplitude across Alaska is in the Supplementary Materials (Figure S22 in Supporting Information S1).

At shorter periods such as 20 s (Figure 3g), the amplitude of Rayleigh wave 4ψ is negligible in central Alaska and largest near the periphery of the study region where uncertainties are largest and observations are less reliable. As period increases (Figures 3h and 4b), the amplitude of Rayleigh wave 4ψ becomes comparable to Love wave 4ψ and at 50 s period it is a bit stronger, on average. As illustrated in Figure 2, Figures S4 and S5 in Supporting Information S1, there are locations and periods where the azimuthal variation of the Rayleigh wave is actually dominated by 4ψ. Figure 4b and also Figures 3c, 3d, 3g, and 3h show that the amplitude of Rayleigh wave 4ψ varies with period more or less opposite from Love wave 4ψ. X. Liu and Ritzwoller (2025) indicate that this is expected in the presence of Rayleigh-Love coupling, where the amplitude of this component of the Love wave, which is stronger at shorter periods, is transmitted to the Rayleigh wave through anisotropy coupling at the longer periods. Ignoring Rayleigh wave 4ψ, for example, can bias estimates of dip angle and ellipticity parameters (X. Liu & Ritzwoller, 2025).

Uncertainty in the fast orientation direction for Rayleigh wave 4ψ is about 10°, which is similar to the uncertainty for Love wave 4ψ. According to X. Liu and Ritzwoller (2025), the sensitivity kernels of Love wave 2ψ and Rayleigh wave 4ψ are basically the same (Figure S23 in Supporting Information S1) as they are both mainly determined by the second term in X (Equation 45 in X. Liu & Ritzwoller, 2025). Therefore, comparing their fast orientations is much more straightforward, compared to comparisons between Love wave 2ψ and Rayleigh wave 2ψ. We find that Rayleigh wave 4ψ fast orientations mainly align with those of Love wave 2ψ (Figure 5e).

Although this is beyond the scope of this paper, we note that inversion tests indicate that strong Rayleigh wave 4ψ at long periods may not be explainable with a TTI mantle, and these observations are more consistent with a tilted orthorhombic elastic tensor in the mantle. A tilted orthorhombic medium in the mantle may further complicate the fast orientations relationships compared with other signals, however.

4. Conclusions

Observations of Rayleigh wave and Love wave 2ψ and 4ψ azimuthal anisotropy are presented here across Alaska at periods ranging from 10 to 50 s based on seismic ambient noise. Here, we address the four questions that motivated this study, with the following conclusions:

1. Both Rayleigh wave 2ψ and Love wave 4ψ are strong across Alaska with the average amplitude of both signals decreasing with period.
2. Love wave 2ψ and Rayleigh wave 4ψ anisotropy also are observed but their average amplitudes grow with period. Love wave 2ψ becomes similar in amplitude to Rayleigh wave 2ψ at the longest periods of this study. Rayleigh wave 4ψ is the weakest of the components studied, but is observable at the longer periods.
3. The fast orientations of several components of anisotropy appear to be related. The mode of the distribution of the difference in fast orientations between the Rayleigh wave 2ψ and Love wave 4ψ is 45 ° and between the Love wave 2ψ and Rayleigh wave 4ψ is 0°. The fast orientation relationship between Rayleigh and Love wave 2ψ is bimodal (0° and 45°–60°), where most differences are in the latter category, which we call quasi-perpendicular. Strike variations of the anisotropic fabric with depth can account for angle differences being substantially different than the expected 0° or 90° for simple seismic models.
4. We interpret the observations of unexpected anisotopy and the complementary amplitude trends of Rayleigh and Love wave 2ψ as well as Rayleigh and Love wave 4ψ to result from Rayleigh-Love coupling becoming stronger at longer periods as the waves become sensitive to the mantle.

We acknowledge that there are physical effects that are not accounted for in this study. For example, finite frequency effects can introduce some theoretical bias into our results such as apparent anisotropy in an isotropic heterogeneous structure (Lin & Ritzwoller, 2011) at longer periods. In addition, strong coupling between Rayleigh and Love waves will cause polarization anomalies that are not accurately accounted for by the tomography methods we apply (eikonal tomography), particularly if the quasi-Rayleigh and quasi-Love waves are not well separated. Nevertheless, attributing all of the unexpected signals to measurement errors, noise, or theoretical bias is implausible, particularly given the systematics that result in the observations. This includes the comparisons between fast orientations and the countervailing amplitude trends of Rayleigh and Love wave components, which we attribute to Rayleigh-Love coupling. Further research about these topics would be worthwhile but is beyond the scope of this paper.

Although earthquake data have been used in many observational studies of azimuthal anisotropy and in some cases in combination with ambient noise, we focus on the interpretation of ambient noise data alone for the following reasons. First, although we find that earthquake data also show strong anisotropy for all four-signals at long periods, especially the unexpected anisotropy, in some regions the anisotropy inferred from earthquake data differs from that based on ambient noise whereas in some regions they are very similar. We think a likely reason for this discrepancy is finite-frequency effects as the sensitivity kernel for earthquake observations are usually much wider than those for ambient noise with uniform noise source distribution. Second, the azimuthal coverage from earthquakes is limited. Third, the waveforms from earthquake data are often very complex. These factors present challenges to observe azimuthal anisotropy reliably from earthquake data, especially for the 4ψ components.

To date, observations of Rayleigh wave 2ψ anisotropy have been the primary data used to infer information about anisotropy from surface waves. Observations of Love wave 2ψ and 4ψ anisotropy as well as Rayleigh wave 4ψ provide new information to improve the inference of the elastic tensor in the crust and mantle in the future in Alaska and presumably in other continents as well.

Conflict of Interest

The authors declare no conflicts of interest relevant to this study.

Data Availability Statement

The network codes for seismic data used in this study include 5C, 7C, 9C, AK, AT, AV, CN, GM, II, IM, IU, PN, PO, PP, TA, US, XE, XF, XI, XN, XR, XV, XY, Y2, YE, YG, YM, YV, ZE, ZQ. DOI for these networks can be found in Table S2 in Supporting Information S1. The dataset of this study is available on Zenodo (X. Liu, 2025, https://zenodo.org/records/17118270). Earthquake Rayleigh wave 2ψ azimuthal anisotropy used in Figure S8 in Supporting Information S1 is available on Zenodo (C. Liu et al., 2022b, https://doi.org/10.5281/zenodo.7080282). Original seismic waveform data were obtained from the Data Management Center of IRIS (www.iris.edu). ObsPy (Beyreuther et al., 2010) is used in data processing. Some figures were made using Generic Mapping Tools (GMT) version 6 (Wessel et al., 2019) licensed under LGPL.

Acknowledgments

We thank two anonymous reviewers, the associate editor, and editor Fenglin Niu for their constructive suggestions, which helped improve the manuscript. XL also thanks Vera Schulte-Pelkum for valuable discussions. The facilities of IRIS Data Services, and specifically the IRIS Data Management Center, were used for access to waveforms, related metadata and/or derived products used in this study. IRIS Data Services are funded through the Seismological Facilities for the Advancement of Geoscience and EarthScope (SAGE) Proposal of the National Science Foundation under Cooperative Agreement EAR-1851048. This study was funded by NSF Grants EAR-1928395 and EAR-1952209 at the University of Colorado Boulder.

References

Backus, G. E. (1965). Possible forms of seismic anisotropy of the uppermost mantle under oceans. *Journal of Geophysical Research*, *70*(14), 3429–3439. https://doi.org/10.1029/JZ070i014p03429

Bensen, G. D., Ritzwoller, M. H., Barmin, M. P., Levshin, A. L., Lin, F., Moschetti, M. P., et al. (2007). Processing seismic ambient noise data to obtain reliable broad-band surface wave dispersion measurements. *Geophysical Journal International*, *169*(3), 1239–1260. https://doi.org/10.1111/j.1365-246x.2007.03374.x

Beyreuther, M., Barsch, R., Krischer, L., Megies, T., Behr, Y., & Wassermann, J. (2010). ObsPy: A Python toolbox for seismology. *Seismological Research Letters*, *81*(3), 530–533. https://doi.org/10.1785/gssrl.81.3.530

Brownlee, S. J., Schulte-Pelkum, V., Raju, A., Mahan, K., Condit, C., & Orlandini, O. F. (2017). Characteristics of deep crustal seismic anisotropy from a compilation of rock elasticity tensors and their expression in receiver functions. *Tectonics*, *36*(9), 1835–1857. https://doi.org/10.1002/2017TC004625

Ekström, G. (2011). A global model of Love and Rayleigh surface wave dispersion and anisotropy, 25-250 s. *Geophysical Journal International*, *187*(3), 1668–1686. https://doi.org/10.1111/j.1365-246X.2011.05225.x

Feng, L., Liu, C., & Ritzwoller, M. H. (2020). Azimuthal anisotropy of the crust and uppermost mantle beneath Alaska. *Journal of Geophysical Research: Solid Earth*, *125*(12), e2020JB020076. https://doi.org/10.1029/2020JB020076

Forsyth, D. W. (1975). The early structural evolution and anisotropy of the oceanic upper mantle. *Geophysical Journal International*, *43*(1), 103–162. https://doi.org/10.1111/j.1365-246X.1975.tb00630.x

Kawakatsu, H. (2016). A new fifth parameter for transverse isotropy. *Geophysical Journal International*, *204*(1), 682–685. https://doi.org/10.1093/gji/ggv479

Lévêque, J. J., Debayle, E., & Maupin, V. (1998). Anisotropy in the Indian Ocean upper mantle from Rayleigh-and love-waveform inversion. *Geophysical Journal International*, *133*(3), 529–540. https://doi.org/10.1046/j.1365-246X.1998.00504.x

Lin, F. C., & Ritzwoller, M. H. (2011). Apparent anisotropy in inhomogeneous isotropic media. *Geophysical Journal International*, *186*(3), 1205–1219. https://doi.org/10.1111/j.1365-246X.2011.05100.x

Lin, F. C., Ritzwoller, M. H., Yang, Y., Moschetti, M. P., & Fouch, M. J. (2011). Complex and variable crustal and uppermost mantle seismic anisotropy in the western United States. *Nature Geoscience*, *4*(1), 55–61. https://doi.org/10.1038/ngeo1036

Liu, C., & Ritzwoller, M. H. (2024). Seismic anisotropy and deep crustal deformation across Alaska. *Journal of Geophysical Research: Solid Earth*, *129*(5), e2023JB028525. https://doi.org/10.1029/2023JB028525

Liu, C., Sheehan, A. F., & Ritzwoller, M. H. (2024). Seismic azimuthal anisotropy beneath the Alaska subduction zone. *Geophysical Research Letters*, *51*(14), e2024GL109758. https://doi.org/10.1029/2024GL109758

Liu, C., Zhang, S., Sheehan, A. F., & Ritzwoller, M. H. (2022a). Surface wave isotropic and azimuthally anisotropic dispersion across Alaska and the Alaska-Aleutian subduction zone. *Journal of Geophysical Research: Solid Earth*, *127*(11), e2022JB024885. https://doi.org/10.1029/2022JB024885

Liu, C., Zhang, S., Sheehan, A. F., & Ritzwoller, M. H. (2022b). Surface wave isotropic and azimuthally anisotropic dispersion across Alaska and the alaska-aleutian subduction Zone [Dataset]. *Zenodo*. https://doi.org/10.5281/zenodo.7080282

Liu, X. (2025). Dataset for rayleigh and love wave Azimuthal Anisotropy based on ambient noise tomography [Dataset]. *Zenodo*. https://doi.org/10.5281/zenodo.17118270

Liu, X., & Ritzwoller, M. H. (2025). The effect of Rayleigh–Love coupling in an anisotropic medium. *Geophysical Journal International*, *241*(2), 1204–1225. https://doi.org/10.1093/gji/ggaf095

Liu, Z., Liang, C., Cao, F., Fan, X., & Chen, C. (2025). Mechanisms for layered anisotropy and anomalous magmatism of Alaska subduction system revealed by ambient noise tomography and the wave gradiometry method. *Journal of Geophysical Research: Solid Earth*, *130*(1), e2024JB029105. https://doi.org/10.1029/2024JB029105

Mauerberger, A., Maupin, V., Gudmundsson, Ó., & Tilmann, F. (2021). Anomalous azimuthal variations with 360° periodicity of Rayleigh phase velocities observed in Scandinavia. *Geophysical Journal International*, *224*(3), 1684–1704. https://doi.org/10.1093/gji/ggaa553

Montagner, J. P., & Jobert, N. (1988). Vectorial tomography—II. Application to the Indian Ocean. *Geophysical Journal International*, *94*(2), 309–344. https://doi.org/10.1111/j.1365-246X.1988.tb05904.x

Montagner, J. P., & Nataf, H. C. (1986). A simple method for inverting the azimuthal anisotropy of surface waves. *Journal of Geophysical Research*, *91*(B1), 511–520. https://doi.org/10.1029/JB091iB01p00511

Montagner, J. P., & Tanimoto, T. (1990). Global anisotropy in the upper mantle inferred from the regionalization of phase velocities. *Journal of Geophysical Research*, *95*(B4), 4797–4819. https://doi.org/10.1029/JB095iB04p04797

Nishimura, C. E., & Forsyth, D. W. (1988). Rayleigh wave phase velocities in the Pacific with implications for azimuthal anisotropy and lateral heterogeneities. *Geophysical Journal International*, *94*(3), 479–501. https://doi.org/10.1111/j.1365-246X.1988.tb02270.x

Polat, G., Lebedev, S., Readman, P. W., O'Reilly, B. M., & Hauser, F. (2012). Anisotropic Rayleigh-wave tomography of Ireland's crust: Implications for crustal accretion and evolution within the Caledonian Orogen. *Geophysical Research Letters*, *39*(4). https://doi.org/10.1029/2012gl051014

Russell, J. B., Gaherty, J. B., Lin, P. Y. P., Lizarralde, D., Collins, J. A., Hirth, G., & Evans, R. L. (2019). High-resolution constraints on Pacific upper mantle petrofabric inferred from surface-wave anisotropy. *Journal of Geophysical Research: Solid Earth*, *124*(1), 631–657. https://doi.org/10.1029/2018JB016598

Schulte-Pelkum, V., Bender, A., & Ruppert, N. A. (2024). Seismicity and anisotropic imaging reveal an active detachment beneath the northern Alaska Range foothills. In *Tectonics and seismic structure of Alaska and Northwestern Canada: EarthScope and beyond (Chapter 21)*. AGU Geophysical Monograph. https://doi.org/10.1002/9781394195947.ch21

Schulte-Pelkum, V., Caine, J. S., Jones III, J. V., & Becker, T. W. (2020). Imaging the tectonic grain of the northern Cordillera orogen using Transportable Array receiver functions. *Seismological Society of America*, *91*(6), 3086–3105. https://doi.org/10.1785/0220200182

Smith, M. L., & Dahlen, F. A. (1973). The azimuthal dependence of Love and Rayleigh wave propagation in a slightly anisotropic medium. *Journal of Geophysical Research*, *78*(17), 3321–3333. https://doi.org/10.1029/JB078i017p03321

Tanimoto, T., & Anderson, D. L. (1985). Lateral heterogeneity and azimuthal anisotropy of the upper mantle: Love and Rayleigh waves 100–250 s. *Journal of Geophysical Research*, *90*(B2), 1842–1858. https://doi.org/10.1029/JB090iB02p01842

Trampert, J., & Woodhouse, J. H. (2003). Global anisotropic phase velocity maps for fundamental mode surface waves between 40 and 150 s. *Geophysical Journal International*, *154*(1), 154–165. https://doi.org/10.1046/j.1365-246X.2003.01952.x

Visser, K., Trampert, J., & Kennett, B. L. N. (2008). Global anisotropic phase velocity maps for higher mode Love and Rayleigh waves. *Geophysical Journal International*, *172*(3), 1016–1032. https://doi.org/10.1111/j.1365-246X.2007.03685.x

Wang, Y., & Tape, C. (2014). Seismic velocity structure and anisotropy of the Alaska subduction zone based on surface wave tomography. *Journal of Geophysical Research: Solid Earth*, *119*(12), 8845–8865. https://doi.org/10.1002/2014JB011438

Wessel, P., Luis, J. F., Uieda, L., Scharroo, R., Wobbe, F., Smith, W. H. F., & Tian, D. (2019). The Generic Mapping Tools version 6. *Geochemistry, Geophysics, Geosystems*, *20*(11), 5556–5564. https://doi.org/10.1029/2019GC008515

Xie, J., Ritzwoller, M. H., Brownlee, S. J., & Hacker, B. R. (2015). Inferring the oriented elastic tensor from surface wave observations: Preliminary application across the western United States. *Geophysical Journal International*, *201*(2), 996–1021. https://doi.org/10.1093/gji/ggv054

Xie, J., Ritzwoller, M. H., Shen, W., & Wang, W. (2017). Crustal anisotropy across eastern Tibet and surroundings modeled as a depth-dependent tilted hexagonally symmetric medium. *Geophysical Journal International*, *209*(1), 466–491. https://doi.org/10.1093/gji/ggx004

Yang, Y. (2021). *Mantle flow systems associated with slab subduction and absolute plate motion in Alaska constrained by shear wave splitting analyses*. Missouri University of Science and Technology.

Yao, H., van Der Hilst, R. D., & Montagner, J. P. (2010). Heterogeneity and anisotropy of the lithosphere of SE Tibet from surface wave array tomography. *Journal of Geophysical Research*, *115*(B12), B12307. https://doi.org/10.1029/2009JB007142

Yuan, H., & Romanowicz, B. (2010). Lithospheric layering in the North American craton. *Nature*, *466*(7310), 1063–1068. https://doi.org/10.1038/nature09332

Yuan, K., & Beghein, C. (2014). Three-dimensional variations in Love and Rayleigh wave azimuthal anisotropy for the upper 800 km of the mantle. *Journal of Geophysical Research: Solid Earth*, *119*(4), 3232–3255. https://doi.org/10.1002/2013JB010853

Zeng, Q., Lin, F. C., & Tsai, V. C. (2024). Spurious Rayleigh-wave apparent anisotropy near major structural boundaries: A numerical and theoretical investigation. *Geophysical Journal International*, *239*(2), 901–913. https://doi.org/10.1093/gji/ggae305

Zhang, S., Feng, L., & Ritzwoller, M. H. (2020). Three-station interferometry and tomography: Coda versus direct waves. *Geophysical Journal International*, *221*(1), 521–541. https://doi.org/10.1093/gji/ggaa046

Zhang, S., Wang, H., Wu, M., & Ritzwoller, M. H. (2021). Isotropic and azimuthally anisotropic Rayleigh wave dispersion across the Juan de Fuca and Gorda plates and US Cascadia from earthquake data and ambient noise two-and three-station interferometry. *Geophysical Journal International*, *226*(2), 862–883. https://doi.org/10.1093/gji/ggab142

Zhu, H., & Tromp, J. (2013). Mapping tectonic deformation in the crust and upper mantle beneath Europe and the North Atlantic Ocean. *Science*, *341*(6148), 871–875. https://doi.org/10.1126/science.1241335

Zhu, H., Yang, J., & Li, X. (2020). Azimuthal anisotropy of the North American upper mantle based on full waveform inversion. *Journal of Geophysical Research: Solid Earth*, *125*(2), e2019JB018432. https://doi.org/10.1029/2019JB018432

References From the Supporting Information

Barmin, M. P., Ritzwoller, M. H., & Levshin, A. L. (2001). A fast and reliable method for surface wave tomography. *Pure and Applied Geophysics*, *158*(8), 1351–1375. https://doi.org/10.1007/PL00001225

Lebigot, E. (2022). Uncertainties: A Python package for calculations with uncertainties, (version 3.17) [Software]. https://uncertainties-python-package.readthedocs.io/en/latest/

Levshin, A. L., Ritzwoller, M. H., Barmin, M. P., Villasenor, A., & Padgett, C. A. (2001). New constraints on the arctic crust and uppermost mantle: Surface wave group velocities, Pn, and Sn. *Physics of the Earth and Planetary Interiors*, *123*(2–4), 185–204. https://doi.org/10.1016/S0031-9201(00)00209-0

Lin, F. C., Ritzwoller, M. H., & Snieder, R. (2009). Eikonal tomography: Surface wave tomography by phase front tracking across a regional broad-band seismic array. *Geophysical Journal International*, *177*(3), 1091–1110. https://doi.org/10.1111/j.1365-246X.2009.04105.x